Cell

CellPress

Article

Metabolic Regulation of the Epigenome Drives Lethal Infantile Ependymoma

Kulandaimanuvel Antony Michealraj,[1,2,28] Sachin A. Kumar,[1,2,3,28] Leo J.Y. Kim,[4,28] Florence M.G. Cavalli,[1,2] David Przelicki,[1,2,3] John B. Wojcik,[5] Alberto Delaidelli,[6,7] Andrea Bajic,[8] Olivier Saulnier,[1,2] Graham MacLeod,[9] Ravi N. Vellanki,[12] Maria C. Vladoiu,[1,2,3] Paul Guilhamon,[1,2] Winnie Ong,[1,2,3] John J.Y. Lee,[1,2,3] Yanqing Jiang,[1,2] Borja L. Holgado,[1,2] Alex Rasnitsyn,[1,2,10] Ahmad A. Malik,[11,17] Ricky Tsai,[11] Cory M. Richman,[1,2,10] Kyle Juraschka,[1,2,3] Joonas Haapasalo,[1,2] Evan Y. Wang,[1,2,10] Pasqualino De Antonellis,[1,2] Hiromichi Suzuki,[1,2] Hamza Farooq,[1,2] Polina Balin,[1,2,3] Kaitlin Kharas,[1,2,3] Randy Van Ommeren,[1,2,3] Olga Sirbu,[1,2,10] Avesta Rastan,[1,2] Stacey L. Krumholtz,[1,2] Michelle Ly,[1,2,3] Moloud Ahmadi,[9] Geneviève Deblois,[12] Dilakshan Srikanthan,[1,2,3] Betty Luu,[1,2] James Loukides,[1,2] Xiaochong Wu,[1,2] Livia Garzia,[13] Vijay Ramaswamy,[1,14] Evgeny Kanshin,[15] María Sánchez-Osuna,[15] Ibrahim El-Hamamy,[16,17] Fiona J. Coutinho,[1,2] Panagiotis Prinos,[18] Sheila Singh,[19,20,21] Laura K. Donovan,[1,2]

(Author list continued on next page)

[1]The Arthur and Sonia Labatt Brain Tumor Research Center, The Hospital for Sick Children, Toronto, ON M5G 0A4, Canada
[2]Developmental & Stem Cell Biology Program, The Hospital for Sick Children, Toronto, ON M5G 0A4, Canada
[3]Department of Laboratory Medicine and Pathobiology, University of Toronto, Toronto, ON M5G 1L7, Canada
[4]Division of Regenerative Medicine, Department of Medicine, University of California, San Diego, La Jolla, CA 92037, USA
[5]Department of Biochemistry and Biophysics and Penn Epigenetics Institute, Perelman School of Medicine, University of Pennsylvania, Philadelphia, PA 19104, USA
[6]Department of Molecular Oncology, British Columbia Cancer Research Centre, Vancouver, BC V6T 1Z2, Canada
[7]Department of Pathology and Laboratory Medicine, University of British Columbia, Vancouver, BC V6T 1Z2, Canada
[8]Department of Human Genetics, McGill University, Montreal, QC H3A 1B1, Canada
[9]Leslie Dan Faculty of Pharmacy, University of Toronto, Toronto, ON M5S 3M2, Canada
[10]Department of Medical Biophysics, University of Toronto, Toronto, ON M5G 1L7, Canada
[11]Centre for Molecular and Systems Biology, Lunenfeld-Tanenbaum Research Institute, Mount Sinai Hospital, Toronto, ON, Canada
[12]Princess Margaret Cancer Centre, University Health Network, Toronto, ON M5G 1L7, Canada
[13]Cancer Research Program, McGill University Health Centre Research Institute, Montreal, QC H4A 3J1, Canada
[14]Division of Haematology/Oncology, Department of Pediatrics, The Hospital for Sick Children, Toronto, ON M5G 1X8, Canada
[15]Institute for Research in Immunology and Cancer (IRIC), Department of Medicine, Université de Montréal, Montréal, QC H3C 3J7, Canada
[16]Computational Biology Program, Adaptive Oncology Theme, Ontario Institute for Cancer Research, Toronto, ON M5G 0A3, Canada

(Affiliations continued on next page)

SUMMARY

Posterior fossa A (PFA) ependymomas are lethal malignancies of the hindbrain in infants and toddlers. Lacking highly recurrent somatic mutations, PFA ependymomas are proposed to be epigenetically driven tumors for which model systems are lacking. Here we demonstrate that PFA ependymomas are maintained under hypoxia, associated with restricted availability of specific metabolites to diminish histone methylation, and increase histone demethylation and acetylation at histone 3 lysine 27 (H3K27). PFA ependymomas initiate from a cell lineage in the first trimester of human development that resides in restricted oxygen. Unlike other ependymomas, transient exposure of PFA cells to ambient oxygen induces irreversible cellular toxicity. PFA tumors exhibit a low basal level of H3K27me3, and, paradoxically, inhibition of H3K27 methylation specifically disrupts PFA tumor growth. Targeting metabolism and/or the epigenome presents a unique opportunity for rational therapy for infants with PFA ependymoma.

INTRODUCTION

Ependymomas are malignant glial tumors that occur throughout the central nervous system (Thompson et al., 2015). Of the nine distinct molecular types of ependymoma, posterior fossa A (PFA) ependymomas, found in the hindbrain of infants and young children, are the most prevalent type (Ramaswamy and Taylor, 2016). The current standard of care is neurosurgical resection followed by radiotherapy, but numerous clinical trials have failed to identify life-extending chemotherapies (Ramaswamy et al.,

Craig Daniels,[1,2] Daniel Schramek,[11,17] Mike Tyers,[15] Samuel Weiss,[22] Lincoln D. Stein,[16,17] Mathieu Lupien,[12] Bradly G. Wouters,[12] Benjamin A. Garcia,[5] Cheryl H. Arrowsmith,[10,12,18] Poul H. Sorensen,[6,7] Stephane Angers,[9,23] Nada Jabado,[8,24] Peter B. Dirks,[1,2,17,25] Stephen C. Mack,[26,*] Sameer Agnihotri,[27,*] Jeremy N. Rich,[4,*] and Michael D. Taylor[1,2,3,10,25,29,*]

[17]Department of Molecular Genetics, University of Toronto, Toronto, ON M5G 1L7, Canada
[18]Structural Genomics Consortium, University of Toronto, 101 College Street, MaRS Centre, South Tower, Toronto, ON M5G 1L7, Canada
[19]Stem Cell and Cancer Research Institute, McMaster University, Hamilton, ON L8S 4K1, Canada
[20]Department of Biochemistry and Biomedical Sciences, McMaster University, Hamilton, ON L8S 4K1, Canada
[21]Department of Surgery, McMaster University, Hamilton, ON L8S 4K1, Canada
[22]Hotchkiss Brain Institute, Department of Cell Biology and Anatomy, Cumming School of Medicine, University of Calgary, Calgary, AB T2N 4N1, Canada
[23]Department of Biochemistry, Faculty of Medicine, University of Toronto, Toronto, ON, Canada
[24]Department of Pediatrics, McGill University, The Research Institute of the McGill University Health Center, Montreal, QC H4A 3J1, Canada
[25]Division of Neurosurgery, The Hospital for Sick Children, Toronto, ON M5G 1L7, Canada
[26]Texas Children's Hospital Cancer Center, Department of Pediatrics, Baylor College of Medicine, Dan L. Duncan Cancer Center, Houston, TX 77030, USA
[27]Department of Neurological Surgery, Children's Hospital of Pittsburgh, University of Pittsburgh School of Medicine, Pittsburgh, PA 15213, USA
[28]These authors contributed equally
[29]Lead Contact
*Correspondence: stephen.mack@bcm.edu (S.C.M.), sameer.agnihotri@gmail.com (S.A.), drjeremyrich@gmail.com (J.N.R.), mdt.cns@gmail.com (M.D.T.)
https://doi.org/10.1016/j.cell.2020.04.047

2016). Up to 40% of children with PFA ependymoma succumb to their disease, and survivors are often left disabled because of toxicity from the tumor and treatment (Ramaswamy and Taylor, 2016).

Unlike most cancers, PFA ependymomas rarely harbor recurrent somatic single-nucleotide variants (sSNVs) or copy number aberrations but, rather, display epigenetic dysregulation, including abnormalities of DNA methylation and histones modifications (Mack et al., 2014; Pajtler et al., 2015). A small minority of PFA tumors harbor somatic mutations in *CXORF67* (*EZHIP*) or *H3F3A* K27M mutations, which have been described previously in diffuse midline gliomas and are associated with histone 3 lysine 27 (H3K27) hypomethylation, which is also observed in PFA tumors (Hübner et al., 2019; Jain et al., 2019; Pajtler et al., 2018; Panwalkar et al., 2017; Ryall et al., 2017).

Research on PFA ependymoma has been hampered because of a lack of representative cell lines, xenografts, or animal models that recapitulate the disease, leading to a lack of therapeutic agents being brought forward to clinical trials (Aldape et al., 2019). We recently demonstrated that the lineage of origin for PFA ependymoma exists only very early in human development, during the first trimester, when the microenvironment of the developing hindbrain is highly hypoxic (Vladoiu et al., 2019). Transcriptional analyses show that PFA ependymomas, but not other molecular ependymoma variants, have elevated hypoxic signaling (Pajtler et al., 2015). Consequently, we hypothesized that the metabolic environment of the developing human fetal hindbrain contributes to PFA ependymomas through intermediary metabolism on the epigenome, offering an opportunity for novel targeted therapy.

RESULTS

Hypoxia Is Essential for PFA Ependymoma Maintenance

To generate patient-derived models, we interrogated the role of oxygen levels in growth of surgical samples of PFA ependymomas. Dissociated single cells (1×10^6) from PFA ependymoma surgical biopsies were cultured under varying oxygen concentrations (21%, 10%, 5%, 1%, and 0.2% O_2). Immediate culture in 1% O_2 allowed establishment of PFA continuous primary cell cultures (9 of 10 specimens), whereas atmospheric O_2 (21%) largely failed (1 of 10, $p = 0.0010$) (Figure 1A). The single PFA culture that was established in 21% O_2 displayed faster growth in 1% O_2 (data not shown). After three generations *in vitro*, PFA cells in 1% versus 21% O_2 proliferated more with decreased markers of cellular senescence ($p21^{WAF1}$) and apoptosis (Annexin V, propidium iodide) (Figures 1B–1G, S1A, and S1B). PFA cells, but not fetal neural stem cells (fNSCs) or supratentorial ependymoma (ST-EPN) cells, underwent G_1 cell cycle arrest after exposure to 21% O_2 ($p = 0.00008$; Figure 1H). PFA cells cultured in 1% versus 21% O_2 displayed increased sphere formation in limiting dilution (Figure S1C). Even short-term exposure (4 days) of PFA cells to 21% O_2 irreversibly inhibited proliferation despite subsequent return to hypoxic conditions (Figure 1I). In a clinical cohort of PFA patients, a hypoxic gene signature informed poor prognosis ($p = 0.00134$) (Figures 1J and S1D). We conclude that maintenance of PFA ependymoma is highly dependent on a hypoxic microenvironment.

PFA Ependymomas Exhibit a Unique Metabolism

Given the association of hypoxia with maintenance of tumorigenesis and modulation of cancer metabolism in tumors, we interrogated six PFA cultures and their corresponding surgical specimens with whole-genome and RNA sequencing (RNA-seq). RNA-seq and proteomics were also compared in three primary cultures grown in 1% and 21% O_2 (Figures 2A, 2B, S2, and S3A–S3E; Tables S1, S2, and S3). Confirming our prior observations (Mack et al., 2014), we did not observe any recurrent sSNVs or copy number aberrations (Figure S2). PFA cells cultured in 1% versus 21% O_2 displayed altered transcription of genes important in regulation of the epigenome (e.g., CXorf67) and metabolism (e.g., *SLC16A3*, *AK4*, and *ALDOC*) (Figure 2A). Mass spectrometry identified a broad set of differentially expressed metabolic

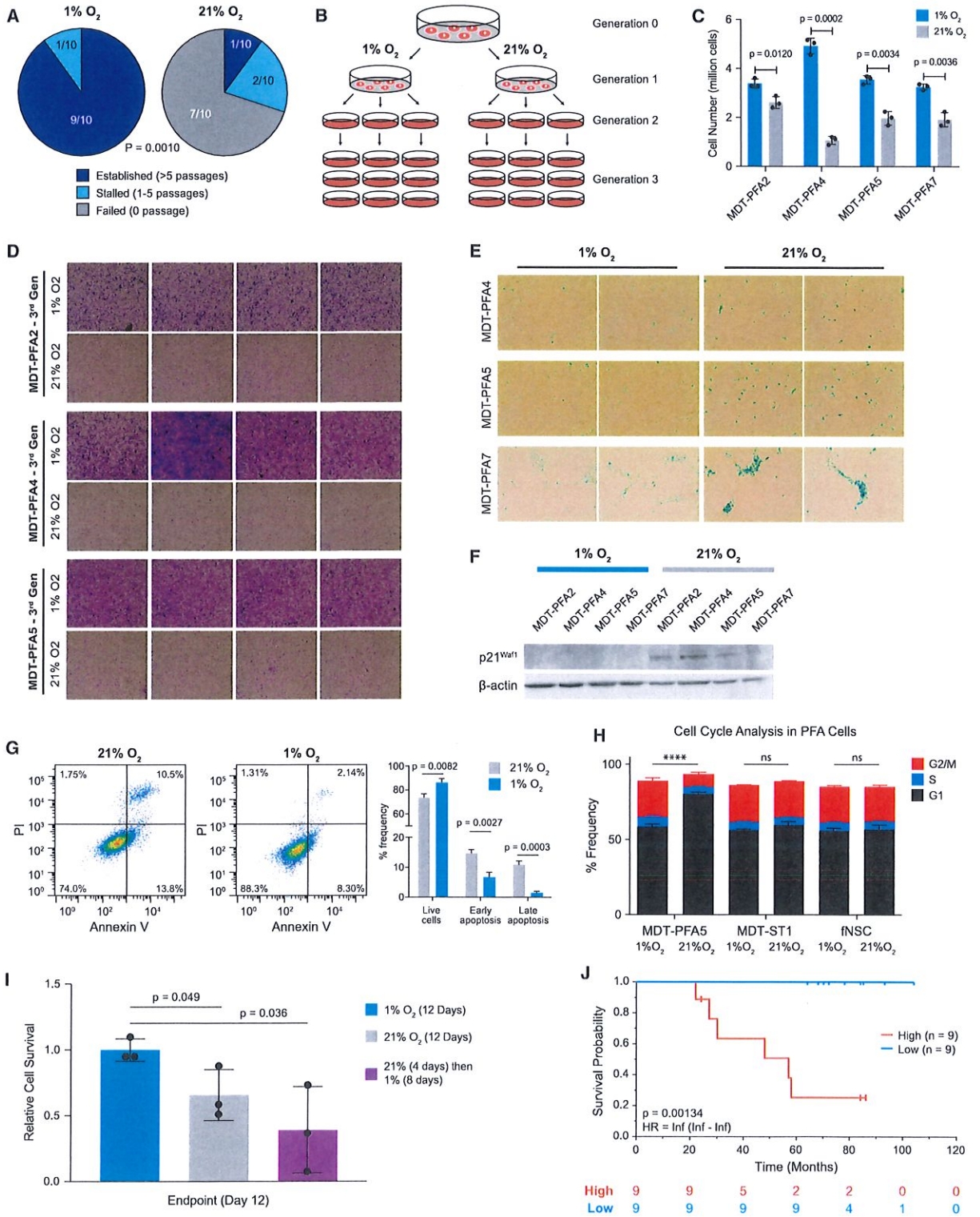

(legend on next page)

enzymes, including LDHA, PGK1, and PFKL (Figure 2B). At the transcriptional and protein levels, hypoxia response and glycolytic metabolism pathways were upregulated in 1% O_2, whereas cellular respiration and electron transport chain genes were increased in 21% O_2. Comparison of the methylation profiles of five primary patient-derived cultures and their parental tissue demonstrated a strong correlation, confirming that cell cultures recapitulate the original tissue (Figure S3F). Mass spectrometry profiling of metabolites from surgical biopsies of 15 PFA ependymomas, 4 ST-EPNs, and 5 normal human pediatric brains demonstrated increased glycolysis, gluconeogenesis and pyruvate metabolism, pentose phosphate metabolism, arginine and proline metabolism, polyamine metabolism, and fatty acid β-oxidation in PFA tissue compared to ST-EPN or normal brain (Figures 2C and S4). Thus, PFA ependymomas have metabolic regulation distinct from other ependymal brain tumors and normal brain.

Hypoxia Regulates the Epigenome of PFA Ependymoma

Leveraging the epigenetic dependencies of PFA ependymomas, we interrogated chromatin regulation of PFA ependymomas under different oxygen conditions by measuring the abundance of all known histone tail post-translational modifications from PFA surgical biopsies as well as PFA cultures in 1% and 21% O_2 using mass spectrometry. PFA surgical biopsies exhibited global loss of H3K27me3 and H3K27me2 with a concomitant increase in H3K27me1 on H3.1/H3.2 and H3.3 histones (Figure 2D). PFA tumors had an increase in H3K27 acetylation compared with ST-EPNs (Figure 2D). PFA ependymomas, but not ST-EPNs or fNSCs, exhibited decreased trimethylation and increased acetylation of histones H3.1 and H3.2 on K27 when grown in 1% O_2 compared with 21% (Figures 2E). To validate these findings, we interrogated surgical ependymoma biopsy specimens for distribution of hypoxia (as measured by immunohistochemical staining of carbonic anhydrase 9 [CA9]) and H3K27me3, demonstrating lower levels of H3K27 trimethylation in the hypoxic regions of PFA ependymoma but not in ST-EPN controls ($p = 0.0195$; Figure S5A). To validate the effect of oxygen tension on H3K27 trimethylation, Cut&Run sequencing was performed. PFA cultures grown in 21% O_2 possessed increased H3K27me3 marks, with changes in promoter silencing corresponding to RNA expression observed above (Figure 2A and S5B–S5D). Collectively, these results show that hypoxia maintains aberrant post-translational modifications of H3K27.

PFA Ependymomas Are Addicted to Glucose

The metabolic profiles of PFA ependymomas suggest that these cells have high levels of glycolysis compared with normal brain or other ependymal tumors (Figures 2C). Stable isotope tracing ($U^{13}C_6$-glucose) gas chromatography-coupled mass spectrometry (GC-MS) demonstrated increased glucose consumption in 1% versus 21% O_2 for PFA cells and other cell types (Figure 2F). However, relative glucose consumption was higher in PFA cells than in ST-EPN cells or fNSCs in 1% O_2 ($p = 0.0212$ and 0.0039, respectively) (Figure 2F). Pharmacologic inhibition of glucose uptake by the glucose transporter GLUT1 using Bay-876 (1 μM) impaired growth of PFA cells compared with ST-EPNs, fNSCs, and diffuse intrinsic pontine glioma (DIPG) cells. (Figure 2G). Glucose supplementation fully rescued the growth defect observed in PFA cells at 21% O_2 (Figure 2H). Thus, high levels of glucose are necessary and sufficient for growth of PFA cells, particularly at increased oxygen levels.

Intermediary Products of PFA Metabolism Regulate Histone Tail Methyltransferase Activity

The hypomethylated and hyperacetylated epigenome observed in PFA ependymoma could be due to various mechanisms of histone modification. The methionine cycle is a key metabolic pathway that provides S-adenosyl methionine (SAM) as a substrate for methylating numerous proteins, including histones. Methionine cycle metabolites, including SAM, were found at similar levels in surgical biopsies of PFA ependymoma and ST-EPN (Figure 3A), but PFA cells cultured at 1% O_2 displayed lower SAM levels compared with cells grown at 21% ($p = 0.0104$), in contrast to ST-EPNs, fNSCs, or immortalized normal human astrocytes (iNHAs) (Figure 3B). Differences in levels of

Figure 1. PFA Ependymoma Mandates Hypoxic Conditions

(A) Patient-derived PFA ependymoma primary cells undergo sustained growth in 1% but not 21% oxygen. Cell lines were considered established when they could sustain 5 consecutive passages in culture, stalled when there were fewer than 5 passages, and failed when they never demonstrated growth *in vitro*. Two-tailed Fisher's exact test was used for statistical comparison.

(B) Schematic representation of continuous culture in 1% versus 21% O_2. A "generation" denotes a consecutive passage under each condition.

(C) Proliferation of PFA cells cultured continuously in 1% O_2 (blue) is significantly sustained and increased compared with 21% O_2 (gray). Cell counts represent average viable cells remaining per plate at the end of the third generation. Statistical comparison was performed using two-tailed t test.

(D) Crystal violet staining of third-generation PFA cells demonstrates high confluence of cells in 1% O_2 compared with 21% O_2. Each square is a representative image of the culture condition.

(E) Senescence-associated β-galactosidase staining of third-generation PFA cells demonstrates increased senescence in 21% O_2 but not 1% O_2. Blue color indicates positive X-gal staining.

(F) Immunoblot for $p21^{Waf1}$ demonstrates increased expression in 21% compared with 1% O_2.

(G) Flow cytometry-based quantification of apoptosis using Annexin V and propidium iodide in PFA cell lines reveals a significant increase in apoptosis in 21% O_2. Statistical comparisons were conducted using Welch's t test from technical triplicates for each sample.

(H) Cell cycle analysis demonstrates an increase in G1 arrest of PFA cells, but not control ST-EPN or fetal neural stem cells (fNSCs), in 21% O_2 versus 1% O_2. Statistical comparison was performed using multiple t testing for the G1 cell cycle phase between 1% versus 21% oxygen of each cell type.

(I) PFA cells cultured in 21% O_2 for 4 days and then returned to 1% O_2 display an irreversible decrease in proliferation. Statistical comparison was performed using two-tailed t test.

(J) Poor outcome among PFA patients with a hypoxic gene signature (MSigDB). The Kaplan-Meier survival curve, stratified by hypoxia signature (high, red; low, blue), is correlated with worse overall survival in a cohort of 18 PFA patients. Statistical comparison was performed using log-rank test after false discovery rate (FDR) correction.

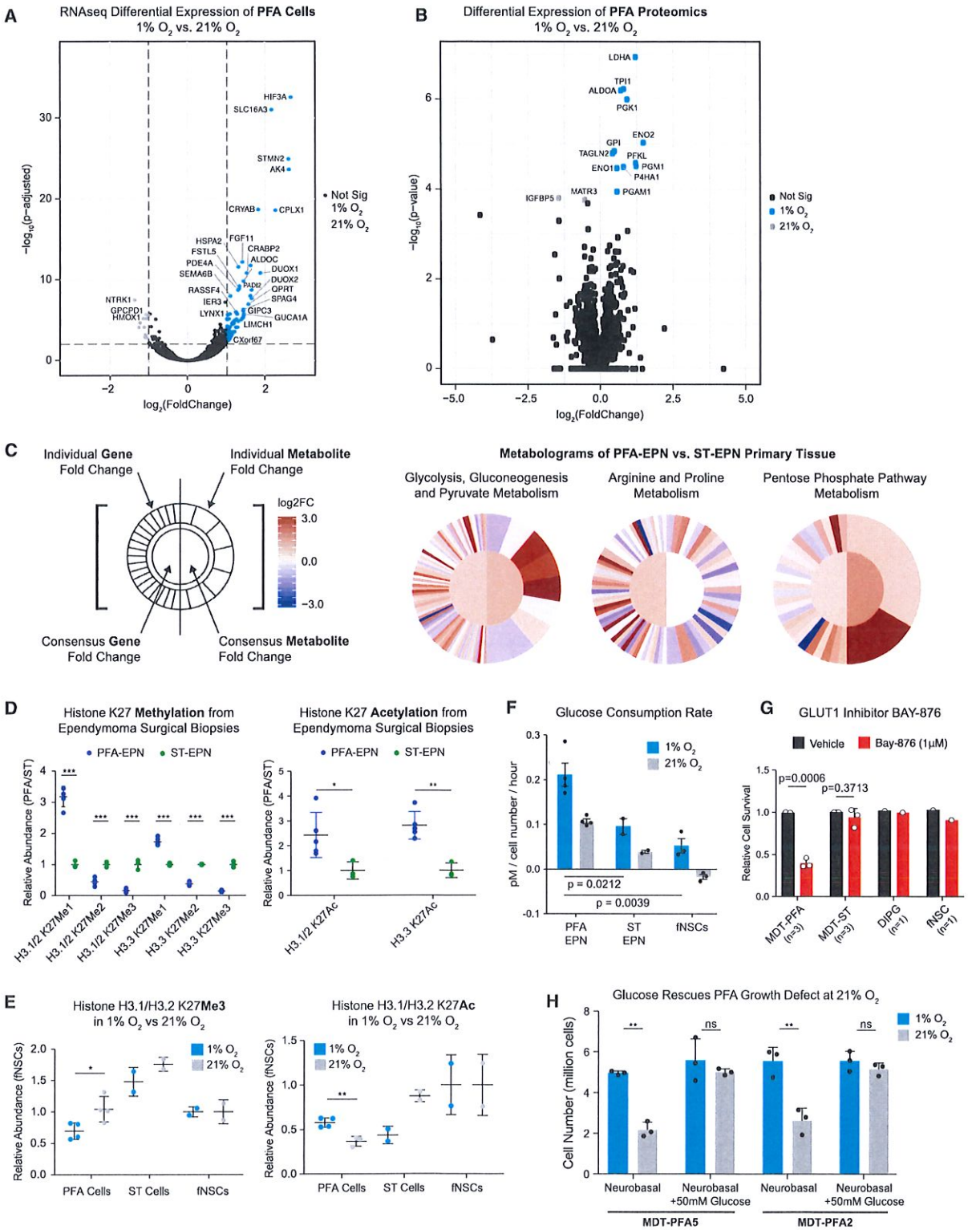

(legend on next page)

H3K27 trimethylation in PFA ependymoma between 1% and 21% O_2 were not due to differences in the expression of core Polycomb Repressive Complex 2 (PRC2) complex genes (*EZH2*, *EED*, or *SUZ12*) (Figure 3C). However, two inhibitors of PRC2 activity, *CXorf67* (*EZHIP*) and *C17orf96* (*EPOP*), displayed elevated levels in PFA cells grown at 1% versus 21% O_2 (Figure 3C; Beringer et al., 2016; Hübner et al., 2019; Jain et al., 2019). Decreased expression of *EZHIP* and *EPOP* in 21% O_2 would be predicted to increase PRC2 activity with consequent increased trimethylation of H3K27. Because SAM is a necessary substrate for the H3K27 methylase EZH2, we hypothesized that increased abundance of SAM in PFA cultures should result in growth inhibition (Figure 3D). Concordantly, exogenous treatment with SAM inhibited growth of PFA cells, but not ST-EPN and iNHA cells, in a concentration-dependent manner (Figure 3E). Endogenous SAM is consumed by two alternate pathways: polyamine metabolism and the nicotinamide sink. SAM is consumed to generate polyamine metabolites through S-adenosylmethionine decarboxylase (SAMDC) activity or sequestered as 1-methylnicotinamide via the enzyme nicotinamide N-methyltransferase (NNMT) (Ulanovskaya et al., 2013). Inhibition of endogenous SAM consumption with sardomozide (a SAMDC inhibitor) or JBSNF-000088 (an NNMT inhibitor) resulted in concentration-dependent growth inhibition of PFA ependymoma cells (Figures 3F and 3G). PFA ependymomas express high levels of the PRC2 inhibitors EZHIP and EPOP *in vitro* and *in vivo*, with reduced levels of the EZH2 substrate SAM *in vitro* under hypoxic conditions, all contributing to maintaining an epigenome with low H3K27me3 levels.

PFA Metabolism Fuels H3K27 Histone Demethylases

The activity of the H3K27 demethylases KDM6A and KDM6B is controlled in part by the concentration of the cofactor α-ketoglutarate (αKG) and in particular by the ratio of αKG to succinate (Carey et al., 2015). The αKG/succinate ratio was much higher in PFA cells than in fNSCs, which decreased when PFA cells were shifted from 1% to 21% O_2 ($p = 0.0040$; Figures 4A and 4B). No differences in the RNA expression levels of *KDM6A* or *KDM6B* were detected under 1% versus 21% O_2 (Figure 4C). $^{13}C_5$-L-glutamine tracing demonstrated that PFA cells preferentially underwent glutaminolysis under reduced Krebs cycle flux, producing αKG from glutamine and maintaining a high αKG/succinate ratio ($p = 0.0023$; Figures 4D and 4E), suggesting potential regulation of demethylase activity rather than total expression. In PFA cells, αKG produced from glutamate (m+5) was highly abundant in 1% O_2 compared with m+3 or m+0 αKG, which were abundant in 21% O_2, consistent with the canonical forward activity of the Krebs cycle in 21% O_2 (Figure S6).

We hypothesized that inhibiting αKG production or histone lysine demethylase (KDM) activity would diminish PFA growth, whereas exogenous αKG should rescue the effects of growth in 21% O_2 (Figure 4F). CB-839, an inhibitor of glutaminolysis, profoundly inhibited growth of PFA cells but not ST-EPN and iNHA cells (Figure 4G). GSK-J4, an inhibitor of the H3K27me3 demethylases KDM6A and KDM6B, demonstrated concentration-dependent growth inhibition of PFA cells but not ST-EPNs or iNHA controls (Figure 4H). Exogenous, αKG rescued the growth defect of PFA cells in 21% O_2 (Figure 4I). To confirm that the inhibition of glutaminolysis by CB-839 was specific to αKG perturbation, we rescued PFA growth with exogenous αKG (Figure 4J). Thus, PFA cells are dependent on H3K27 demethylase activity maintained through a high αKG/succinate ratio generated by glutaminolysis and reduced Krebs cycle flux.

PFA Undergoes Reductive Carboxylation to Generate Acetyl-CoA, Fueling H3K27 Acetylation

Acetylation of H3K27 blocks the ability of EZH2 to methylate H3K27. Histone acetyltransferase (HAT) complexes consume acetyl-coenzyme A (CoA), a product of intermediary metabolism, to acetylate histone tails. PFA surgical biopsies have very high levels of H3K27 acetylation that diminish upon exposure to 21% O_2 (Figures 2D and 2E). The αKG/citrate ratio is a marker of reductive carboxylation, which results in production of acetyl-CoA from citrate (Fendt et al., 2013; Lee et al., 2014). In PFA cells, but not fNSCs, the αKG/citrate ratio was higher in 1% versus 21% O_2 (Figures 5A and 5B). Expression of the HAT complex genes *CREBBP* and *EP300* was unchanged between 1% and 21% O_2 (Figure 5C).

We hypothesized that high levels of acetyl-CoA production could drive H3K27 acetylation in PFA cells. $^{13}C_5$-L-glutamine tracing demonstrated that, in PFA cells, citrate was primarily produced by reductive carboxylation (m+5, m+3) in 1% O_2, whereas citrate was consumed by forward activity of the Krebs cycle (m+4) in 21% O_2 ($p < 0.0001$; Figures 5D, 5E, and S5). Production

Figure 2. PFA Ependymomas Harbor a Unique Metabolic and Global Histone Hypomethylation Profile

(A) Volcano plot of differential gene expression analysis for PFA cells cultured in 1% versus 21% oxygen. Significantly differentially expressed genes are indicated in color (log_2fold change > 1, $P_{adj} < 0.05$).

(B) Volcano plot of differential proteomic expression analysis for PFA cells cultured in 1% O_2 versus 21% O_2. Significantly differentially expressed proteins are indicated in color (FDR < 0.05).

(C) Integrative metabologram of gene expression and metabolite abundance for selected KEGG pathways in PFA tissue relative to ST-EPN tissue (derived from Hakimi et al. 2016). Log_2fold change is shown on a set scale from −3.0 to 3.0.

(D) Relative levels of histone K27 methylation and acetylation in PFA (n = 5) versus ST-EPN surgical (n = 3) biopsies assessed by post-translational modification histone-tail mass spectrometry.

(E) Relative abundance of H3.1 and H3.2 K27 methylation and acetylation in cultured PFA, ST, and (fNSCs) under 1% and 21% O_2, as assessed by post-translational modification histone-tail mass spectrometry.

(F) Increased glucose consumption rate of cultured PFA cells compared with ST and fNSCs and in 1% versus 21% O_2.

(G) Treatment of PFA cells with a GLUT1-specific inhibitor, BAY-876 (1 μM), perturbs PFA cell but not ST-EPN, fNSC, or DIPG survival in 1% O_2. The bar plot shows relative survival.

(H) Glucose (50 mM) supplementation rescues the growth defect of third-generation PFA cells grown in 21% O_2.

Data are displayed as mean ± SEM. *$p < 0.05$, **$p < 0.01$, and ***$p < 0.001$. Statistical comparisons were conducted using Welch's t test for (D)–(H).

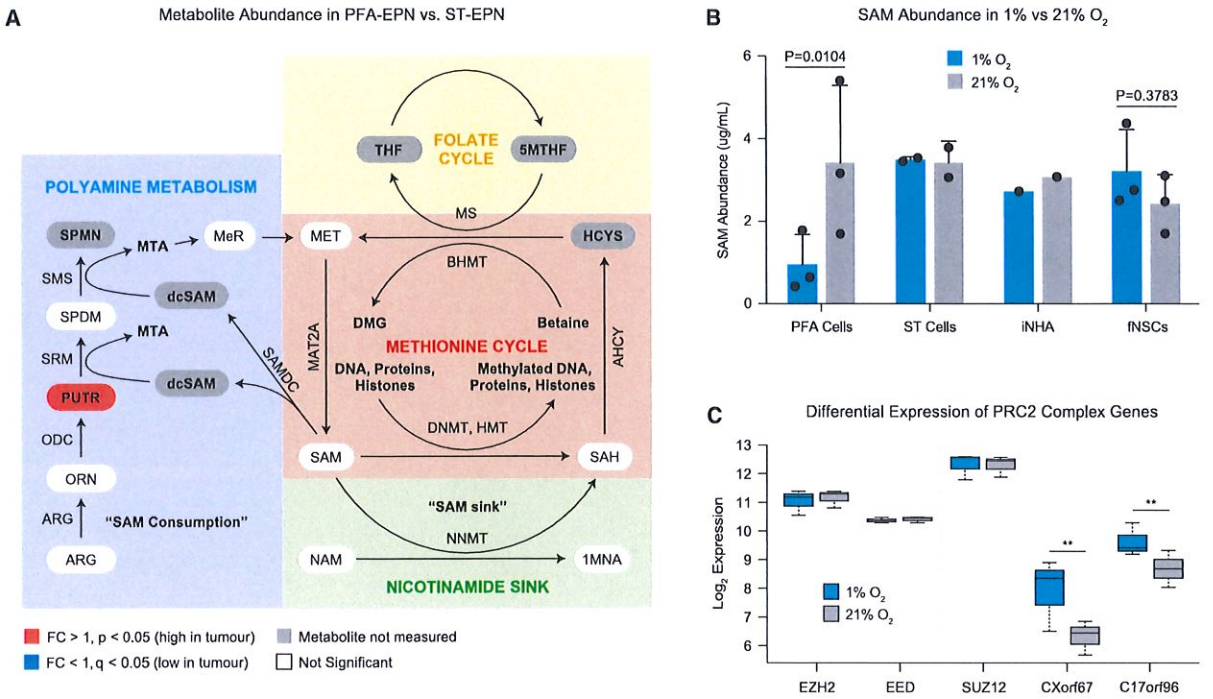

(legend on next page)

of cytosolic fumarate, malate, and aspartate (m+3) was detected in 1% O_2 (Figure S7), which are produced when ATP citrate lyase (ACLY) converts citrate into acetyl-CoA. Thus, PFA ependymoma cells, but not ST-EPNs or fNSCs, consume glutamate and undergo reductive carboxylation, resulting in high levels of acetyl-CoA (Figures 5D, 5E, and S7). To test the functional relevance of our metabolic model, we determined the activity of P300/CREBBP acetyltransferase inhibitors and ACLY inhibitors against PFA ependymoma cells (Figure 5F). The P300 complex inhibitor A485 demonstrated concentration-dependent inhibition of PFA cell growth in contrast to ST-EPNs or iNHAs (Figure 5G). A485 treatment caused limited growth inhibition of diffuse intrinsic pontine glioma (DIPG) cells, a tumor type that similarly exhibits genome-wide H3K27 hypomethylation. In orthogonal experiments, pharmacologic inhibition of production of acetyl-CoA from citrate using the ACLY inhibitor BMS-303141 diminished growth of PFA cells but not ST-EPNs (Figure 5H). Blockade of ACLY can force cells to utilize external sources of acetate to create acetyl-coA via intracellular acetyl-CoA synthetases (Gao et al., 2016); exogenous acetate rescued the growth of PFA cells treated with the ACLY inhibitor in a concentration-dependent manner (Figure 5I). Consistent with our proposed model, supplementation of PFA cells with exogenous acetate rescued the growth inhibition mediated by the glutaminase inhibitor CB-839 (Figure 5J). Collectively, we conclude that glutaminolysis, followed by reductive carboxylation, generates high levels of acetyl-CoA to maintain increased H3K27Ac.

Basal PRC2 Activity Is Essential for PFA Survival—the PFA Goldilocks Model

We leveraged the ability to culture PFA cells to perform a genome-wide CRISPR knockout screen to identify essential genes in three patient-derived PFA cell cultures compared with another malignant brain cancer, glioblastoma (GBM) (Figure 6A; MacLeod et al., 2019). PFA cultures had a total of 272 context-specific fitness genes (Z score < 0.05, average PFA Bayes factor > 4, average GBM Bayes factor < 4) (Table S4). Three of the top 10 essential genes specific to PFA ependymoma were EED, SUZ12, and EZH2, all core components of PRC2 (Figure 6A). Essential genes specific to PFA ependymoma by pathway analysis focused on histone lysine methylation (Figure 6A). The essentiality of PRC2 genes in PFA seems paradoxical because our results above suggest that increasing H3K27 trimethylation decreases the fitness of PFA ependymoma (Figures 3, 4, and 5), but although PFA cells are hypomethylated at H3K27, they display basal H3K27 trimethylation. We compared our PFA CRISPR screens with previously published screens of human fNSCs (Table S5; MacLeod et al., 2019). A total of 316 essential genes were observed, with 128 genes overlapping with the PFA versus GBM comparison (Table S6). These results suggest that a minimal basal level of H3K27me3 is essential for PFA survival and that further attenuation of H3K27me3 decreases the fitness of PFA ependymoma cells. PFA cells have a unique epigenome, suggesting a model in which they thrive in a narrow Goldilocks zone, with deviation to increased or decreased H3K27me3 levels leading to diminished cellular fitness (Figure 6B).

Our results demonstrated that interventions regulating H3K27 methylation, demethylation, or acetylation that increase H3K27me3 levels diminish the fitness of PFA cells. To test our Goldilocks model, we inhibited H3K27 trimethylation through inhibition of SAM production using PF9366, an inhibitor of MAT2A, the enzyme responsible for generating SAM. PFA cells, but not other brain cell types, treated with PF9366 demonstrated inhibition of cell growth (Figure 6C). Inhibition of the PRC2 component EED using A395, but not the inactive control probe, diminished the growth of PFA cells (Figure 6D). Similarly, EZH2 inhibition using the compound UNC1999 readily inhibited PFA growth compared with other control lines (Figure 6E). Therefore, inhibition of production of the methyl donor SAM or of the activity of the PRC2 complex (through EED or EZH2) supports our Goldilocks model of the PFA epigenome.

Normal Fetal Hindbrain Cells in the PFA Lineage of Origin Have a Hypoxic Phenotype

PFA ependymoma is a glial tumor that arises very early in the fetal gliogenic lineage from gliogenic progenitors and roof plate-like stem cells (Vladoiu et al., 2019). Murine roof plate-like stem cells were almost exclusively present at embryonic day 10 (E10), whereas gliogenic progenitors had peak prevalence at E16 (Figure 7A). Single-cell RNA-seq data from different time points across murine hindbrain development demonstrated that hypoxia gene expression signatures correspond to the peak prevalence of these two cell populations (Figure 7B). Pathway analysis revealed that E16 gliogenic progenitors displayed strong transcriptional signatures of glycolysis, gluconeogenesis, and monosaccharide metabolism, similar to the transcriptome of PFA ependymoma, but post-natal day 0 (P0) gliogenic progenitors upregulated genes associated with the electron transport chain and cellular respiration pathways (Figure 7C). Because PFA ependymomas have a very low mutational burden and resemble normal fetal hindbrain cells, we hypothesized that the

Figure 3. Hypoxia Drives SAM Deficiency, Perturbing PRC2-Dependent Methylation and Maintaining H3K27 Hypomethylation in PFA Ependymoma

(A) Relative metabolite abundance of methionine cycle metabolites and intermediates, including the NNMT sink and polyamine metabolism, in PFA (n = 15) versus ST-EPN (n = 4) surgical biopsies. Significantly differentially abundant metabolites were characterized by t test with FDR correction (q < 0.05).

(B) Hypoxia significantly decreases SAM abundance in PFA cells but not control ST-EPN cells, immortalized normal human astrocytes (iNHAs), or fNSCs. Statistical comparison was performed using ratio-paired t test.

(C) Hypoxia does not affect the transcript expression of PRC2 core subunits but does increases the expression of the PRC inhibitory genes CXorf67 (EZHIP) and C17orf96 (EPOP) in 1% oxygen. Statistical comparison was performed using Wald test with Benjamini-Hochberg adjustment.

(D) Cartoon depicting the relationship between metabolism of SAM (SAM-consuming metabolic pathways) and PRC2 complex activity during K27 methylation. Hypoxia-mediated overexpression of PRC2 complex inhibitory genes (blue) and targets/drugs (red) are indicated.

(E) Supplementing exogenous SAM to PFA cells grown in 1% O_2 diminishes survival in a dose-dependent manner.

(F) Dose-dependent sardomozide inhibition (7 days) of SAM decarboxylation (polyamine metabolism) diminishes PFA cell survival in 1% O_2.

(G) Dose-dependent JBSNF-000088 inhibition (7 days) of the NNMT (methylation) sink perturbs PFA cell survival in 1% O_2.

*p < 0.05 and **p < 0.01. Data are displayed as the mean ± SEM. Curves show logistic regression line of fit for (E)–(G).

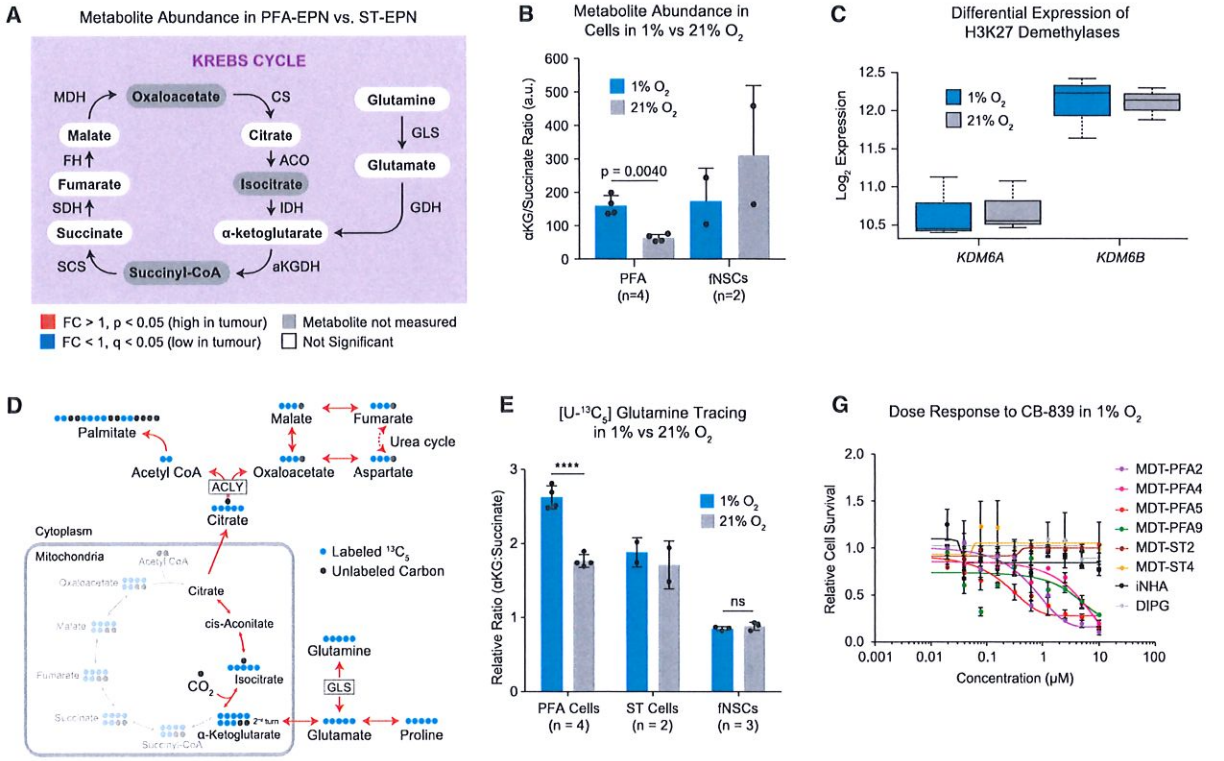

(legend on next page)

metabolic microenvironment of the hindbrain in early development would resemble PFA metabolism. Whole mouse hindbrain tissue was isolated from E16 and P2. A total of 19 metabolites that were enriched in PFA compared with ST-EPN tissue (Table S7) were identified in the mouse hindbrain samples. Unsupervised clustering of metabolites exhibited an enrichment at E16 compared with P2, concordant with PFAs arising early in cerebellar development (Figure 7D). We conclude that the unique metabolic phenotype of PFA ependymoma mirrors metabolic changes in the gliogenic lineage of the developing hindbrain.

DISCUSSION

Pediatric brain tumors, including lethal midline glioma, medulloblastoma, atypical teratoid rhabdoid tumors (ATRT), and ependymomas, reflect the epigenetic developmental states of their cells of origin (Mack et al., 2016). *IDH* mutant astrocytomas in young adults have previously demonstrated a link between metabolism and the epigenome in neuro-oncology (Parsons et al., 2008). We now identify a metabolic-epigenomic link in PFA ependymomas that informs the phenotype of PFA ependymoma and possible development of novel therapeutic strategies for these lethal cancers.

A diverse array of normal stem cells and cancer cells preferentially grows in hypoxia, but PFA ependymoma cells appear to be unique in that they are permanently poisoned after only transient exposure to room air. Future work to isolate and study the lineage of origin will determine whether the unique metabolism of PFA cells merely reflects their cells of origin in the early hindbrain or is an acquired phenotype. The specific roles of metabolic factors, including hypoxia, acute or chronic, during fetal development in development of PFA ependymoma awaits robust prospective *in vivo* investigation in model organisms.

The occurrence of PFA ependymoma in the hypoxic hindbrain during fetal and early post-natal life controls the availability of the intermediary products of metabolism, including SAM (which regulates histone methylation), α-KG (which regulates histone demethylation), and acetyl-CoA (which regulates histone acetylation), collectively resulting in H3K27 hypomethylation. Comparisons of metabolite abundance from primary PFA tissues did not provide the resolution to identify the enrichment or depletion of key metabolites that we observed in primary cultures. This is likely a limitation of bulk PFA tissues, which contain contaminating immune cells and stromata, and highlights the importance of *in vitro* primary cell culture models to decipher such phenotypes (Vladoiu et al., 2019).

Pharmacologic agents targeting selected metabolites or the resulting histone post-translational modification displayed specific activity against PFAs. Although the PFA ependymoma epigenome exhibits marked global H3K27 hypomethylation, the residual levels of H3K27 trimethylation were critical for cell survival, leading to the seemingly paradoxical finding that inhibition or potentiation of PRC2 complex activity profoundly reduces the fitness of PFA cells, suggesting broad utility as a targeted therapy.

PFA ependymoma is a very unusual malignancy of infancy, with a paucity of known recurrent somatic mutations, in which microenvironmental regulation of the epigenome appears to play a major role in tumorigenesis. Targeting the highly tuned availability of metabolic intermediates as well as the finely balanced epigenome should be evaluated for children with PFA ependymoma.

STAR★METHODS

Detailed methods are provided in the online version of this paper and include the following:

- KEY RESOURCES TABLE
- RESOURCE AVAILABILITY
  - Lead Contact
  - Materials Availability
  - Data and Code Availability
- EXPERIMENTAL MODEL AND SUBJECT DETAILS
  - Patient derived PFA and ST Tissue
  - Patient derived PFA and ST Cell Cultures
  - Mouse Housing and Husbandry
- METHOD DETAILS
  - Primary Cell Culture Establishment
  - Growth Curve/Proliferation Analysis
  - Cell Confluence Analysis
  - Senescence β-Galactosidase Staining

Figure 4. Hypoxia Maintains Histone Lysine Demethylase Activity by Increasing αKG Abundance via Glutaminolysis in PFA Ependymoma

(A) Snapshot of relative metabolite abundance of Krebs cycle intermediates in PFA (n = 15) versus ST-EPN (n = 4) surgical biopsies. Significantly differentially abundant metabolites were characterized by t test with FDR correction ($q < 0.05$).

(B) PFA cells growing in 1% O_2, exhibit a significantly increased ratio of αKG/succinate in PFA cells. Statistical comparison was performed using ratio-paired t test.

(C) Histone lysine 27 demethylase gene expression is not differentially regulated by oxygen tension in PFA cells. Statistical comparison was performed using Wald test with Benjamini-Hochberg adjustment.

(D) Cartoon depicting glutamine tracing in PFA cells growing in 1% O_2. Labeled glutamine was used as the carbon source ($^{13}C_5$, light blue; unlabeled carbon, dark blue). PFA cells preferentially undergo glutaminolysis and reductive carboxylation.

(E) Labeled glutamine tracing of PFA cells reveals an elevated αKG/succinate ratio in 1% compared with 21% O_2. Statistical analysis was performed using two-tailed t test with Holm-Sidak correction.

(F) Cartoon depicting the roles of αKG and the KDMs in histone demethylation. Drugs that inhibit lysine 27 demethylase activity and their targets are shown in red, whereas exogenous αKG, which increases activity, is shown in green.

(G) Dose response of GSK-J4 inhibition (7 days) of KDM6A and KDM6B perturbs PFA cell survival in 1% O_2.

(H) Dose response of CB-839 inhibition (7 days) of GLS perturbs PFA cell survival in 1% O_2.

(I) Supplementing exogenous cell-permeable dimethyl αKG rescues the growth defect of PFA cells cultured in 21% O_2. Statistical comparison using unpaired two-tailed t test with Welch's correction.

(J) Supplementing exogenous cell-permeable dimethyl αKG rescues PFA cell survival while under CB-839 inhibition in 1% O_2. Statistical comparison conducted using multiple t tests with Holm-Sidak correction.

*$p < 0.05$, **$p < 0.01$, and ****$p < 0.0001$. Data are displayed as the mean ± SEM. Curves show logistic regression line of fit for (G) and (H).

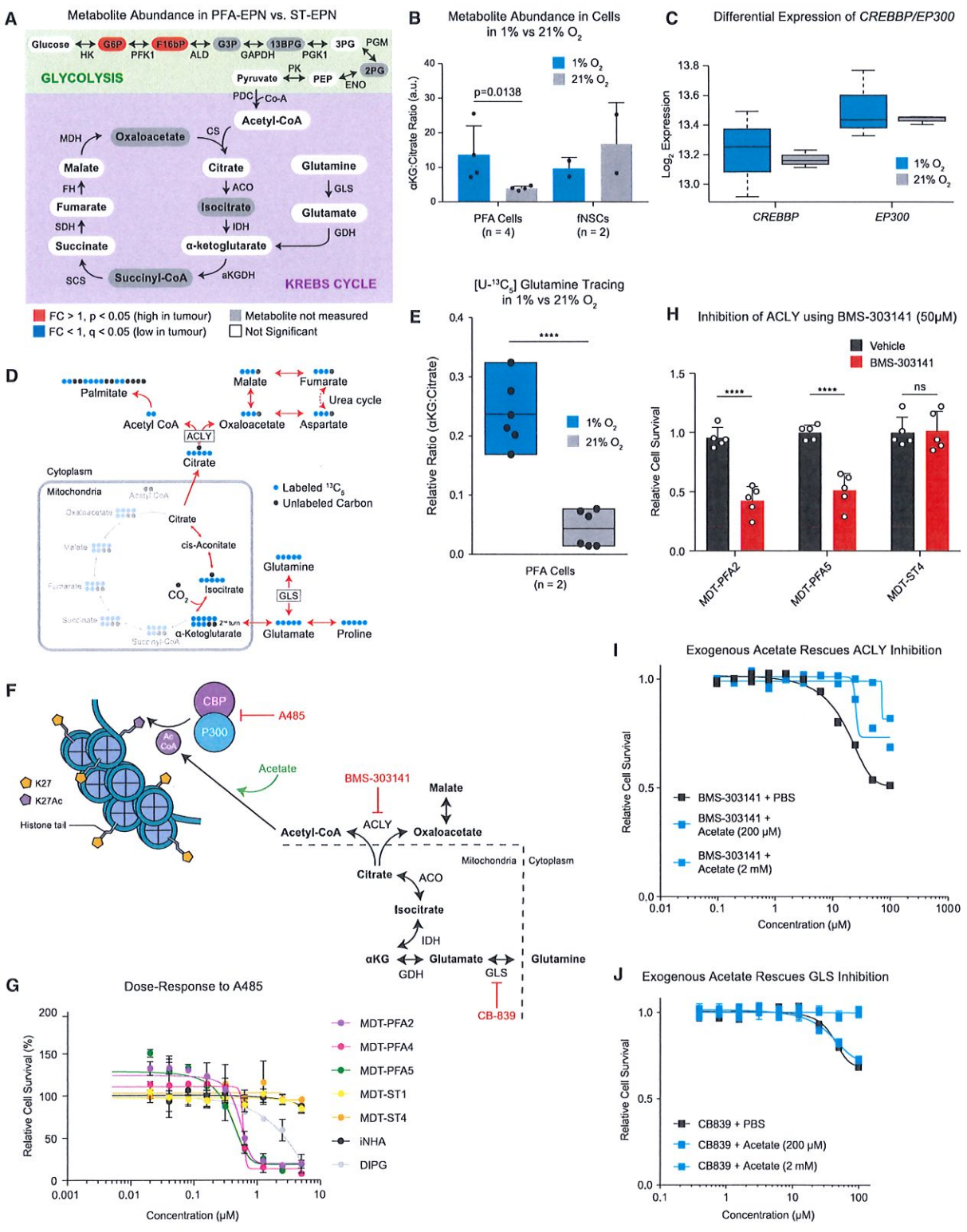

(legend on next page)

- Apoptosis and Cell Cycle Analysis
- Western Blotting
- Transient Growth in 21% Oxygen
- *In Vitro* Limiting Dilution Analysis (LDAs)
- Co-isolation of DNA and RNA
- WGS Library Preparation
- RNAseq Library Preparation
- Proteomics
- Histone extraction and Histone tail PTM mass spectrometry analysis
- S-Adenosylmethionine (SAM) quantitation
- Cell viability assay
- Immunohistochemistry (IHC) and analysis
- Metabolite extraction, derivatization, gas chromatography/mass spectrometry
- Extracellular Flux and Glucose/Glutamine Consumption Rate Measurements
- Glucose rescue
- Dimethyl alpha-Ketoglutarate Rescue of Normoxia and GLS inhibition
- Acetate rescue of ACLY or GLS inhibition
- Single Cell RNAseq
- Genome-wide knockout screen
- Cut&Run Sequencing
- Metabolomics
- Ultrahigh Performance Liquid Chromatography-Tandem Mass Spectroscopy (UPLC-MS/MS)

- QUANTIFICATION AND STATISTICAL ANALYSIS
  - Survival Analysis Stratified by Hypoxia Gene Signature
  - Bulk RNA-sequencing Data Pre-Processing
  - Whole-Genome Sequencing Data Pre-Processing and Somatic Mutation Assessment
  - Analysis of 850K methylation data comparing PFA tissue & cell line
  - Proteomics
  - Single Cell RNaseq
  - Analysis of genome-wide CRISPR screen data
  - Analysis of Cut&Run Sequencing Data for H3K27 trimethylation
  - Global metabolite profiling by Metabolon Inc
- ADDITIONAL RESOURCES

SUPPLEMENTAL INFORMATION

Supplemental Information can be found online at https://doi.org/10.1016/j.cell.2020.04.047.

ACKNOWLEDGMENTS

This work was supported by National Institutes of Health grants CA203101 (to L.J.Y.K.); CA197718, CA154130, CA169117, CA171652, CA238662, NS087913, NS103434, and NS089272 (to J.N.R.); and CA148699 and CA159859 (to M.D.T.). M.D.T. is also supported by a Stand Up To Cancer (SU2C) St. Baldrick's Pediatric Dream Team translational research grant (SU2C-AACR-DT1113) and SU2C Canada Cancer Stem Cell Dream Team research funding (SU2C-AACR-DT-19-15) provided by the Government of Canada through Genome Canada and the Canadian Institutes of Health Research, with supplementary support from the Ontario Institute for Cancer Research through funding provided by the Government of Ontario. SU2C is a program of the Entertainment Industry Foundation administered by the American Association for Cancer Research. M.D.T. is also supported by the Pediatric Brain Tumor Foundation, the Terry Fox Research Institute, the Canadian Institutes of Health Research, the Cure Search Foundation, b.r.a.i.n.child, Meagan's Walk, the SWIFTY Foundation, the Brain Tumour Charity, Genome Canada, Genome BC, Genome Quebec, the Ontario Research Fund, Worldwide Cancer Research, the V-Foundation for Cancer Research, and the Ontario Institute for Cancer Research through funding provided by the Government of Ontario. Additionally, M.D.T. is supported by a Canadian Cancer Society Research Institute Impact grant, a Cancer Research UK Brain Tumour Award, the Garron Family Chair in Childhood Cancer Research at the Hospital for Sick Children, and the University of Toronto. The authors would also like to thank Meera Kamal (administrative assistant) and James Loukides (Tumour Bank manager) and recognize the Labatt Brain Tumour Research Centre and the Michael and Amira Dan Brain Tumour Bank Network. We would also like to acknowledge the Isla Kerr Fund for continued support of ependymoma research at SickKids. K.A.M. is supported by a MITACS ELEVATE postdoctoral fellowship. S.A.K. is supported by a ResTraComp doctoral scholarship, the Hospital for Sick Children, the McLaughlin Centre, the University of Toronto, and the Ruggles Family Foundation, University of Toronto. S.C.M. is supported by a Cancer Prevention Research Institute of Texas (CPRIT) scholar award (RR170023), an Alex's Lemonade Stand Foundation (ALSF) A award and Young Investigator award, a Pediatric Brain Tumor Foundation award, a Chad Tough Young Investigator award, a Cookies for Cancer research grant, a RALLY research grant, a BEAR Necessities Pediatric Cancer Foundation grant, a Children's Cancer Research Fund award, a Children's Brain Tumor Foundation award, and a Baylor College of Medicine Junior Faculty award. The SGC is a registered charity (number 1097737) that receives funds from AbbVie, Bayer Pharma AG, Boehringer Ingelheim, the Eshelman Institute for Innovation, Genome Canada through the Ontario Genomics Institute (OGI-055), the Innovative Medicines Initiative (EU/EFPIA) (ULTRA-DD grant 115766), Janssen,

Figure 5. Hypoxia Drives Reverse TCA Cycle Activity to Increase Histone K27 Acetylation in PFA Ependymoma

(A) Relative metabolite abundance of Krebs cycle and glycolysis intermediates in PFA (n = 15) versus ST-EPN (n = 4) surgical biopsies. Significantly differentially abundant metabolites were characterized by t test with FDR correction ($q < 0.05$).

(B) The αKG/citrate ratio is significantly lower in PFA cells in 21% versus 1% oxygen, which is not mirrored in fNSCs. Statistical comparison was performed using ratio-paired t test.

(C) Expression of the lysine acetyltransferase components CREBBP and p300 is not influenced by oxygen tension in PFA cells. Statistical comparison was performed using Wald test with Benjamini-Hochberg adjustment.

(D) Cartoon depicting glutamine tracing in PFA cells growing in 1% O_2. Labeled glutamine was used as the carbon source ($^{13}C_5$, light blue; unlabeled carbon, dark blue). PFA cells preferentially undergo glutaminolysis and reductive carboxylation.

(E) Labeled glutamine tracing of PFA cells demonstrates an increased aKG/citrate ratio, a marker of reductive carboxylation, in 1% O_2. Statistical analysis was performed using two-tailed t test with Holm-Sidak correction.

(F) Cartoon depicting the roles of acetate and lysine 27 acetyltransferases in histone acetylation. Drugs that inhibit lysine 27 acetyltransferase activity and their targets are shown in red, whereas exogenous acetate, which increases activity, is shown in green.

(G) Dose-dependent selective inhibition (7 days) of CREBBP/P300 by A485 diminishes PFA cell survival at 1% O_2.

(H) BMS-303141 (50 μM) inhibition (7 days) of ACLY diminishes PFA cell survival in 1% O_2. Statistical analysis was performed by t test with Welch's correction.

(I) Addition of exogenous acetate (200 μM and 2mM) rescues BMS-303141 inhibition of ACLY in PFA cells in 1% O_2.

(J) Addition of exogenous acetate (200 μM and 2mM) rescues CB-839 inhibition of GLS in PFA cells in 1% O_2.

****$p < 0.0001$. Data are displayed as the mean ± SEM. Curves show logistic regression line of fit for (G), (I), and (J).

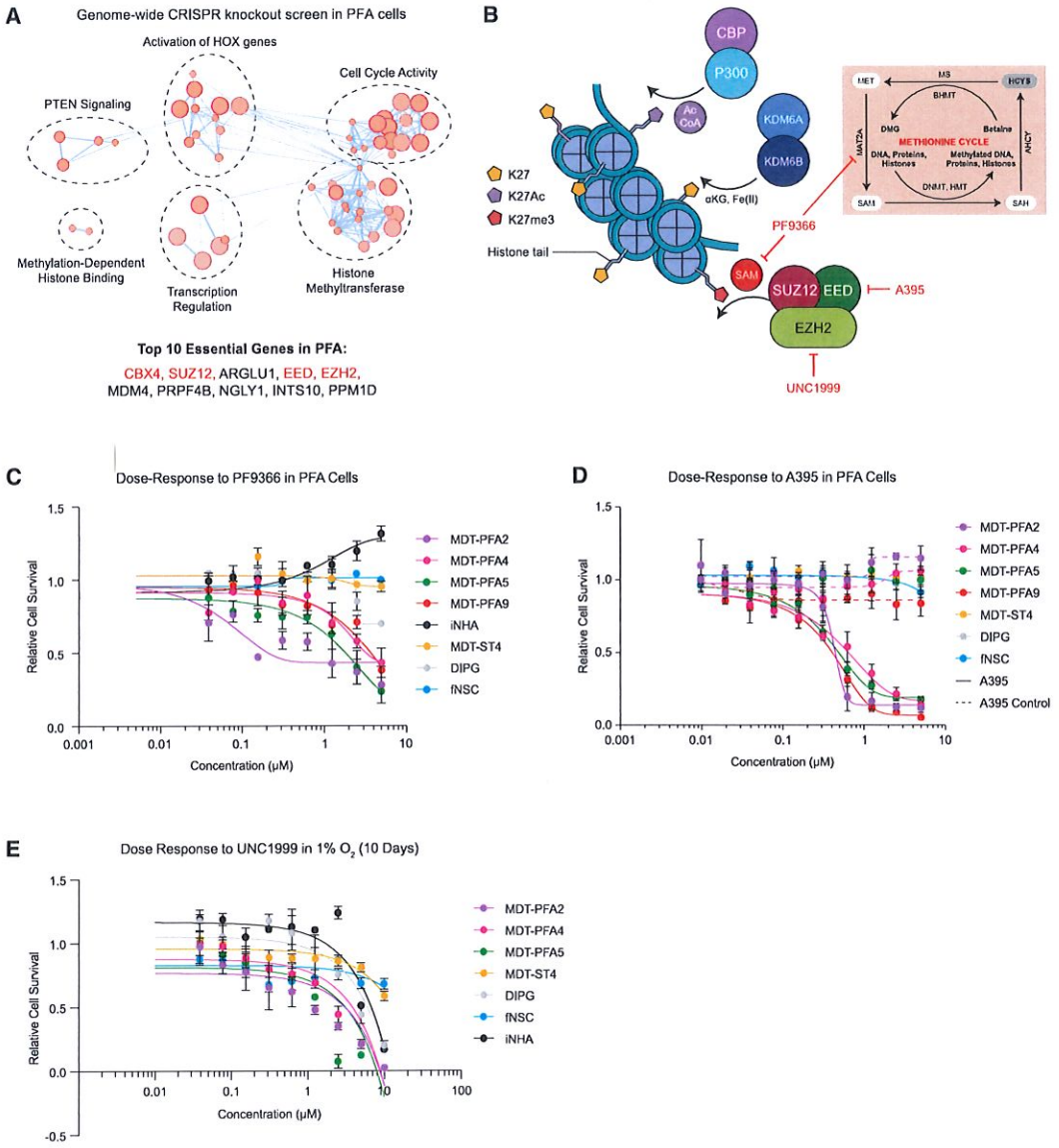

Figure 6. Paradoxically, Inhibition of the PRC2 Complex Also Shows Activity against PFA Ependymoma

(A) Pathway analysis of significantly essential genes by genome-wide CRISPR knockout essentiality screen in PFA cells compared with GBM cells (*Z* score, $p < 0.05$). The top 10 hits ranked by average difference of quantile normalized Bayes factor between PFA and GBM screens are listed. Genes associated with the PRC2 complex are denoted in red.

(B) Cartoon depicting several mechanisms of K27 modification active in PFA ependymoma. Targeted inhibition of MAT2A by PF9366 and the PRC2 complex components EED and EZH2 by A395 and UNC1999, respectively, are depicted.

(C) Dose-dependent inhibition (7 days) of MAT2A by PF9366 inhibits SAM production, resulting in diminished PFA cell survival, while simultaneously augmenting iNHA control cell survival in 1% O_2. ST, DIPG, and fNSC control lines showed no effect upon treatment.

(D) Dose-dependent inhibition (7 days) of EED by A395 diminishes PFA cell survival in 1% O_2. An inactive analog of the A395 probe (dashed) did not affect PFA cell survival. ST, DIPG, and fNSC control lines showed no effect upon treatment.

(E) Dose-dependent inhibition (10 days) of EZH2 by UNC1999 diminishes PFA cell survival in 1% O_2. ST, DIPG, and fNSC control lines showed no effect upon treatment.

Curves show logistic regression line of fit for (C)–(E).

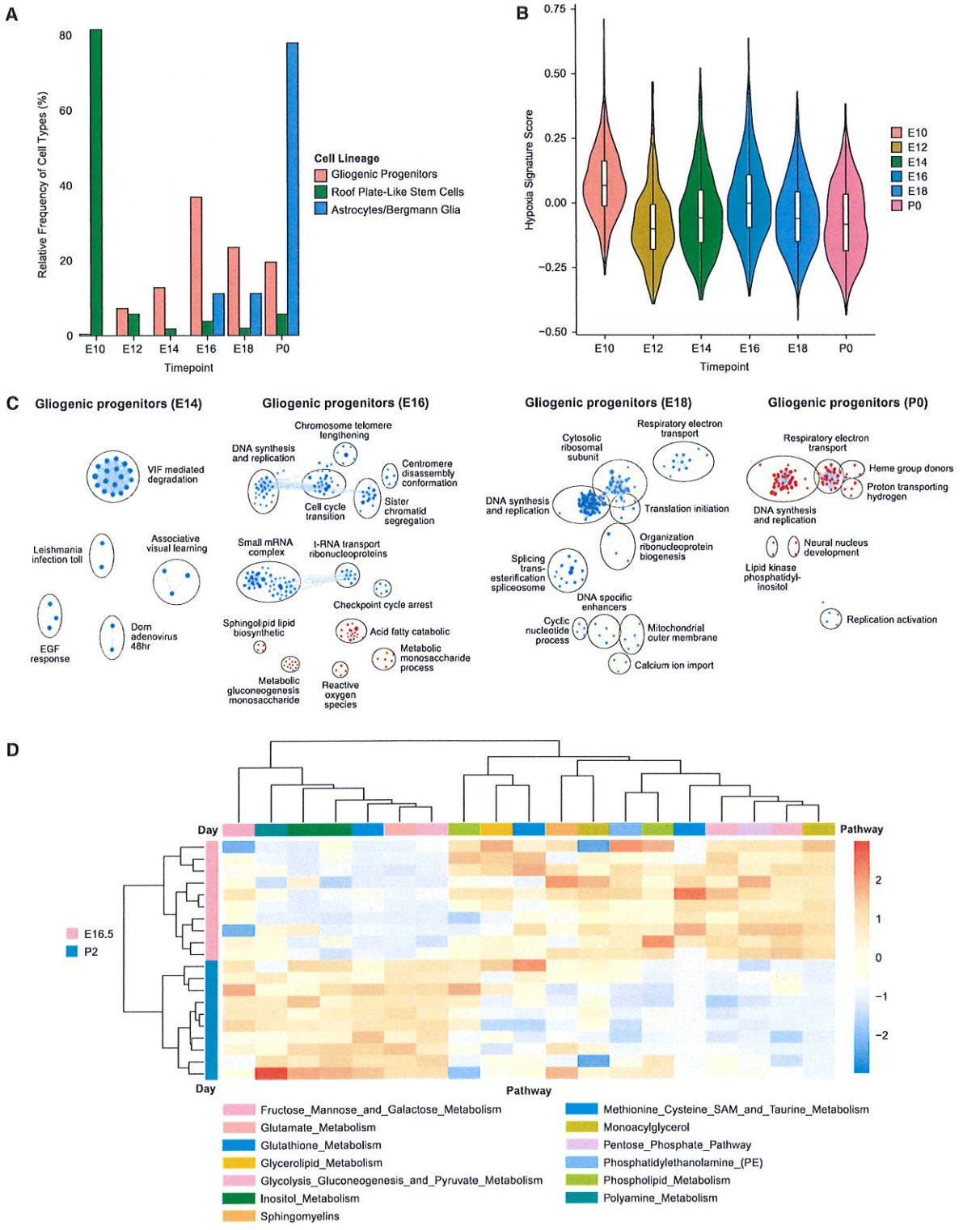

(legend on next page)

Merck KGaA (Darmstadt, Germany), MSD, Novartis Pharma AG, Pfizer, the São Paulo Research Foundation-FAPESP, Takeda, and Wellcome.

AUTHOR CONTRIBUTIONS

Conceptualization, K.A.M., S.A.K., L.J.Y.K., S.C.M., S. Agnihotri, J.N.R., and M.D.T.; Methodology, K.A.M., S.A.K., L.J.Y.K., S.C.M., S. Agnihotri, J.N.R., and M.D.T.; Validation, K.A.M., S.A.K., and L.J.Y.K.; Formal Analysis, F.M.G.C., O. Saulnier, M.C.V., P.G., A. Rasnitsyn, A.A.M., E.Y.W., H.S., H.F., and I.E.-H.; Investigation, K.A.M., S.A.K., L.J.Y.K., D.P., J.B.W., A.D., A.B., G.M., R.N.V., W.O., J.J.Y.L., Y.J., B.L.H., R.T., C.M.R., K.J., J.H., P.D.A., P.B., K.K., R.V.O., O. Sirbu, M. Ly, M.A., G.D., D. Srikanthan, L.K.D., and E.K.; Resources, B.L., J.L., and F.J.C.; Data Curation, F.M.G.C., O. Saulnier, P.G., A. Rasnitsyn, A.A.M., H.S., and H.F.; Writing – Original Draft, K.A.M., S.A.K., L.J.Y.K., S.C.M., S. Agnihotri, J.N.R., and M.D.T.; Writing – Reviewing & Editing, K.A.M., S.A.K., L.J.Y.K., S.C.M., S. Agnihotri, J.N.R., and M.D.T.; Visualization, A. Rastan and S.L.K.; Supervision, L.G., V.R., P.P., S.S., D. Schramek, M.T., S.W., L.D.S., M. Lupien, B.G.W., B.A.G., C.H.A., P.H.S., S. Angers, N.J., P.B.D., S.C.M., S. Agnihotri, J.N.R., and M.D.T.; Project Administration, X.W. and C.D.; Funding Acquisition, S.C.M., S. Agnihotri, J.N.R., and M.D.T.

DECLARATION OF INTERESTS

The authors declare no competing interests.

Received: September 27, 2019
Revised: March 16, 2020
Accepted: April 24, 2020
Published: May 22, 2020

REFERENCES

Aldape, K., Brindle, K.M., Chesler, L., Chopra, R., Gajjar, A., Gilbert, M.R., Gottardo, N., Gutmann, D.H., Hargrave, D., Holland, E.C., et al. (2019). Challenges to curing primary brain tumours. Nat. Rev. Clin. Oncol. *16*, 509–520.

Amemiya, H.M., Kundaje, A., and Boyle, A.P. (2019). The ENCODE Blacklist: Identification of Problematic Regions of the Genome. Sci. Rep. *9*, 9354–9355.

Andrews, S. (2010). FastQC: a quality control tool for high throughput sequence data (Babraham Bioinformatics).

Badur, M.G., Muthusamy, T., Parker, S.J., Ma, S., McBrayer, S.K., Cordes, T., Magana, J.H., Guan, K.-L., and Metallo, C.M. (2018). Oncogenic R132 IDH1 Mutations Limit NADPH for De Novo Lipogenesis through (D)2-Hydroxyglutarate Production in Fibrosarcoma Sells. Cell Rep. *25*, 1018–1026.e4.

Beringer, M., Pisano, P., Di Carlo, V., Blanco, E., Chammas, P., Vizán, P., Gutiérrez, A., Aranda, S., Payer, B., Wierer, M., and Di Croce, L. (2016). EPOP Functionally Links Elongin and Polycomb in Pluripotent Stem Cells. Mol. Cell *64*, 645–658.

Buffa, F.M., Harris, A.L., West, C.M., and Miller, C.J. (2010). Large meta-analysis of multiple cancers reveals a common, compact and highly prognostic hypoxia metagene. Br. J. Cancer *102*, 428–435.

Carey, B.W., Finley, L.W.S., Cross, J.R., Allis, C.D., and Thompson, C.B. (2015). Intracellular α-ketoglutarate maintains the pluripotency of embryonic stem cells. Nature *518*, 413–416.

Chi, J.-T., Wang, Z., Nuyten, D.S.A., Rodriguez, E.H., Schaner, M.E., Salim, A., Wang, Y., Kristensen, G.B., Helland, A., Børresen-Dale, A.-L., et al. (2006). Gene expression programs in response to hypoxia: cell type specificity and prognostic significance in human cancers. PLoS Med. *3*, e47.

Cibulskis, K., Lawrence, M.S., Carter, S.L., Sivachenko, A., Jaffe, D., Sougnez, C., Gabriel, S., Meyerson, M., Lander, E.S., and Getz, G. (2013). Sensitive detection of somatic point mutations in impure and heterogeneous cancer samples. Nat. Biotechnol. *31*, 213–219.

Connor, A.A., Denroche, R.E., Jang, G.H., Lemire, M., Zhang, A., Chan-Seng-Yue, M., Wilson, G., Grant, R.C., Merico, D., Lungu, I., et al. (2019). Integration of Genomic and Transcriptional Features in Pancreatic Cancer Reveals Increased Cell Cycle Progression in Metastases. Cancer Cell *35*, 267–282.e7.

Cox, J., and Mann, M. (2008). MaxQuant enables high peptide identification rates, individualized p.p.b.-range mass accuracies and proteome-wide protein quantification. Nat. Biotechnol. *26*, 1367–1372.

Dobin, A., Davis, C.A., Schlesinger, F., Drenkow, J., Zaleski, C., Jha, S., Batut, P., Chaisson, M., and Gingeras, T.R. (2013). STAR: ultrafast universal RNA-seq aligner. Bioinformatics *29*, 15–21.

Fan, Y., Xi, L., Hughes, D.S.T., Zhang, J., Zhang, J., Futreal, P.A., Wheeler, D.A., and Wang, W. (2016). MuSE: accounting for tumor heterogeneity using a sample-specific error model improves sensitivity and specificity in mutation calling from sequencing data. Genome Biol. *17*, 178.

Fardin, P., Barla, A., Mosci, S., Rosasco, L., Verri, A., and Varesio, L. (2009). The *l1-l2* regularization framework unmasks the hypoxia signature hidden in the transcriptome of a set of heterogeneous neuroblastoma cell lines. BMC Genomics *10*, 474.

Favaro, E., Lord, S., Harris, A.L., and Buffa, F.M. (2011). Gene expression and hypoxia in breast cancer. Genome Med. *3*, 55.

Favero, F., Joshi, T., Marquard, A.M., Birkbak, N.J., Krzystanek, M., Li, Q., Szallasi, Z., and Eklund, A.C. (2015). Sequenza: allele-specific copy number and mutation profiles from tumor sequencing data. Ann. Oncol. *26*, 64–70.

Fendt, S.-M., Bell, E.L., Keibler, M.A., Olenchock, B.A., Mayers, J.R., Wasylenko, T.M., Vokes, N.I., Guarente, L., Vander Heiden, M.G., and Stephanopoulos, G. (2013). Reductive glutamine metabolism is a function of the α-ketoglutarate to citrate ratio in cells. Nat. Commun. *4*, 2236.

Gao, X., Lin, S.-H., Ren, F., Li, J.-T., Chen, J.-J., Yao, C.-B., Yang, H.-B., Jiang, S.-X., Yan, G.-Q., Wang, D., et al. (2016). Acetate functions as an epigenetic metabolite to promote lipid synthesis under hypoxia. Nat. Commun. *7*, 11960.

Gaspar, J.M. (2018). Improved peak-calling with MACS2. bioRxiv. https://doi.org/10.1101/496521.

Hakimi, A.A., Reznik, E., Lee, C.-H., Creighton, C.J., Brannon, A.R., Luna, A., Aksoy, B.A., Liu, E.M., Shen, R., Lee, W., et al. (2016). An Integrated Metabolic Atlas of Clear Cell Renal Cell Carcinoma. Cancer Cell *29*, 104–116.

Harris, B.H.L., Barberis, A., West, C.M.L., and Buffa, F.M. (2015). Gene Expression Signatures as Biomarkers of Tumour Hypoxia. Clin. Oncol. (R. Coll. Radiol.) *27*, 547–560.

Hart, T., Chandrashekhar, M., Aregger, M., Steinhart, Z., Brown, K.R., MacLeod, G., Mis, M., Zimmermann, M., Fradet-Turcotte, A., Sun, S., et al. (2015). High-Resolution CRISPR Screens Reveal Fitness Genes and Genotype-Specific Cancer Liabilities. Cell *163*, 1515–1526.

Figure 7. The Normal Glial Lineage of Origin of PFA in the Hindbrain Displays Early Hypoxia during Normal Development

(A) Relative frequency of gliogenic progenitors and roof-plate like stem cells across several embryonic time points. Frequency is calculated as the number of cells of that type at each time point relative to the total number of cells of that type across all time points.

(B) Violin plot of the signature score for hypoxia genes across the embryonic time points. The hypoxia signature set is based on 15 genes (*Aldoa*, *Aldoc*, *Bnip3*, *Bnip3l*, *Car9*, *Ddit4*, *Gpi1*, *Ldha*, *P4ha1*, *P4ha2*, *Pdk1*, *Pgk1*, *Tpi1*, *Vegfa*, and *Zfp395*). Set scale from −1 to 1.

(C) Gene set enrichment analysis of mouse cerebellar gliogenic progenitors across four developmental time points, generated from single-cell RNA-seq (scRNA-seq). Cytoscape maps were generated using $q < 0.15$ and $p < 0.05$.

(D) Heatmap of PFA enriched metabolites demonstrates a higher correlation to E16.5 compared with P2 embryonic time points. A total of 19 significantly enriched metabolites in PFA ependymoma tissue (FDR < 0.05, fold change > 0) were assessed in mouse hindbrain tissue isolated at E16.5 and P2 embryonic time points. Normalized metabolite abundance was plotted with a set scale of 3 to −3. Annotations of metabolic KEGG pathways are indicated for reference.

Hart, T., and Moffat, J. (2016). BAGEL: a computational framework for identifying essential genes from pooled library screens. BMC Bioinformatics *17*, 164–167.

Hu, Y., and Smyth, G.K. (2009). ELDA: extreme limiting dilution analysis for comparing depleted and enriched populations in stem cell and other assays. J. Immunol. Methods *347*, 70–78.

Hübner, J.-M., Müller, T., Papageorgiou, D.N., Mauermann, M., Krijgsveld, J., Russell, R.B., Ellison, D.W., Pfister, S.M., Pajtler, K.W., and Kool, M. (2019). EZHIP/CXorf67 mimics K27M mutated oncohistones and functions as an intrinsic inhibitor of PRC2 function in aggressive posterior fossa ependymoma. Neuro-oncol. *21*, 878–889.

Jain, S.U., Do, T.J., Lund, P.J., Rashoff, A.Q., Diehl, K.L., Cieslik, M., Bajic, A., Juretic, N., Deshmukh, S., Venneti, S., et al. (2019). PFA ependymoma-associated protein EZHIP inhibits PRC2 activity through a H3 K27M-like mechanism. Nat. Commun. *10*, 2146.

Josephidou, M., Lynch, A.G., and Tavaré, S. (2015). multiSNV: a probabilistic approach for improving detection of somatic point mutations from multiple related tumour samples. Nucleic Acids Res. *43*, e61.

Kim, D., Langmead, B., and Salzberg, S.L. (2015). HISAT: a fast spliced aligner with low memory requirements. Nat. Methods *12*, 357–360.

Koboldt, D.C., Zhang, Q., Larson, D.E., Shen, D., McLellan, M.D., Lin, L., Miller, C.A., Mardis, E.R., Ding, L., and Wilson, R.K. (2012). VarScan 2: somatic mutation and copy number alteration discovery in cancer by exome sequencing. Genome Res. *22*, 568–576.

Kondo, S., Kubota, S., Mukudai, Y., Moritani, N., Nishida, T., Matsushita, H., Matsumoto, S., Sugahara, T., and Takigawa, M. (2006). Hypoxic regulation of stability of connective tissue growth factor/CCN2 mRNA by 3′-untranslated region interacting with a cellular protein in human chondrosarcoma cells. Oncogene *25*, 1099–1110.

Koong, A.C., Denko, N.C., Hudson, K.M., Schindler, C., Swiersz, L., Koch, C., Evans, S., Ibrahim, H., Le, Q.T., Terris, D.J., and Giaccia, A.J. (2000). Candidate genes for the hypoxic tumor phenotype. Cancer Res. *60*, 883–887.

Lee, J.V., Carrer, A., Shah, S., Snyder, N.W., Wei, S., Venneti, S., Worth, A.J., Yuan, Z.-F., Lim, H.-W., Liu, S., et al. (2014). Akt-dependent metabolic reprogramming regulates tumor cell histone acetylation. Cell Metab. *20*, 306–319.

Lewis, C.A., Parker, S.J., Fiske, B.P., McCloskey, D., Gui, D.Y., Green, C.R., Vokes, N.I., Feist, A.M., Vander Heiden, M.G., and Metallo, C.M. (2014). Tracing compartmentalized NADPH metabolism in the cytosol and mitochondria of mammalian cells. Mol. Cell *55*, 253–263.

Li, H., and Durbin, R. (2010). Fast and accurate long-read alignment with Burrows-Wheeler transform. Bioinformatics *26*, 589–595.

Li, H., Handsaker, B., Wysoker, A., Fennell, T., Ruan, J., Homer, N., Marth, G., Abecasis, G., and Durbin, R.; 1000 Genome Project Data Processing Subgroup (2009). The Sequence Alignment/Map format and SAMtools. Bioinformatics *25*, 2078–2079.

Li, W., Xu, H., Xiao, T., Cong, L., Love, M.I., Zhang, F., Irizarry, R.A., Liu, J.S., Brown, M., and Liu, X.S. (2014). MAGeCK enables robust identification of essential genes from genome-scale CRISPR/Cas9 knockout screens. Genome Biol. *15*, 554.

Liberzon, A., Birger, C., Thorvaldsdóttir, H., Ghandi, M., Mesirov, J.P., and Tamayo, P. (2015). The Molecular Signatures Database Hallmark Gene Set Collection. Cell Systems *1*, 417–425.

Love, M.I., Huber, W., and Anders, S. (2014). Moderated estimation of fold change and dispersion for RNA-seq data with DESeq2. Genome Biol. *15*, 550.

Mack, S.C., Witt, H., Piro, R.M., Gu, L., Zuyderduyn, S., Stütz, A.M., Wang, X., Gallo, M., Garzia, L., Zayne, K., et al. (2014). Epigenomic alterations define lethal CIMP-positive ependymomas of infancy. Nature *506*, 445–450.

Mack, S.C., Hubert, C.G., Miller, T.E., Taylor, M.D., and Rich, J.N. (2016). An epigenetic gateway to brain tumor cell identity. Nat. Neurosci. *19*, 10–19.

MacLeod, G., Bozek, D.A., Rajakulendran, N., Monteiro, V., Ahmadi, M., Steinhart, Z., Kushida, M.M., Yu, H., Coutinho, F.J., Cavalli, F.M.G., et al. (2019). Genome-Wide CRISPR-Cas9 Screens Expose Genetic Vulnerabilities and Mechanisms of Temozolomide Sensitivity in Glioblastoma Stem Cells. Cell Rep. *27*, 971–986.e9.

Maina, E.N., Morris, M.R., Zatyka, M., Raval, R.R., Banks, R.E., Richards, F.M., Johnson, C.M., and Maher, E.R. (2005). Identification of novel VHL target genes and relationship to hypoxic response pathways. Oncogene *24*, 4549–4558.

Manalo, D.J., Rowan, A., Lavoie, T., Natarajan, L., Kelly, B.D., Ye, S.Q., Garcia, J.G.N., and Semenza, G.L. (2005). Transcriptional regulation of vascular endothelial cell responses to hypoxia by HIF-1. Blood *105*, 659–669.

Merico, D., Isserlin, R., Stueker, O., Emili, A., and Bader, G.D. (2010). Enrichment map: a network-based method for gene-set enrichment visualization and interpretation. PLoS ONE *5*, e13984.

Mootha, V.K., Lindgren, C.M., Eriksson, K.-F., Subramanian, A., Sihag, S., Lehar, J., Puigserver, P., Carlsson, E., Ridderstråle, M., Laurila, E., et al. (2003). PGC-1alpha-responsive genes involved in oxidative phosphorylation are coordinately downregulated in human diabetes. Nat. Genet. *34*, 267–273.

Pajtler, K.W., Witt, H., Sill, M., Jones, D.T.W., Hovestadt, V., Kratochwil, F., Wani, K., Tatevossian, R., Punchihewa, C., Johann, P., et al. (2015). Molecular Classification of Ependymal Tumors across All CNS Compartments, Histopathological Grades, and Age Groups. Cancer Cell *27*, 728–743.

Pajtler, K.W., Wen, J., Sill, M., Lin, T., Orisme, W., Tang, B., Hübner, J.-M., Ramaswamy, V., Jia, S., Dalton, J.D., et al. (2018). Molecular heterogeneity and CXorf67 alterations in posterior fossa group A (PFA) ependymomas. Acta Neuropathol. *136*, 211–226.

Panwalkar, P., Clark, J., Ramaswamy, V., Hawes, D., Yang, F., Dunham, C., Yip, S., Hukin, J., Sun, Y., Schipper, M.J., et al. (2017). Immunohistochemical analysis of H3K27me3 demonstrates global reduction in group-A childhood posterior fossa ependymoma and is a powerful predictor of outcome. Acta Neuropathol. *134*, 705–714.

Parsons, D.W., Jones, S., Zhang, X., Lin, J.C.-H., Leary, R.J., Angenendt, P., Mankoo, P., Carter, H., Siu, I.-M., Gallia, G.L., et al. (2008). An integrated genomic analysis of human glioblastoma multiforme. Science *321*, 1807–1812.

Ramaswamy, V., and Taylor, M.D. (2016). Treatment implications of posterior fossa ependymoma subgroups. Chin. J. Cancer *35*, 93–94.

Qi, J., Nakayama, K., Cardiff, R.D., Borowsky, A.D., Kaul, K., Williams, R., Krajewski, S., Mercola, D., Carpenter, P.M., and Bowtell, D. (2010). Siah2-Dependent Concerted Activity of HIF and FoxA2 Regulates Formation of Neuroendocrine Phenotype and Neuroendocrine Prostate Tumors. Cancer Cell *18*, 23–38.

Quinlan, A.R., and Hall, I.M. (2010). BEDTools: a flexible suite of utilities for comparing genomic features. Bioinformatics *26*, 841–842.

Ramaswamy, V., Hielscher, T., Mack, S.C., Lassaletta, A., Lin, T., Pajtler, K.W., Jones, D.T.W., Luu, B., Cavalli, F.M.G., Aldape, K., et al. (2016). Therapeutic Impact of Cytoreductive Surgery and Irradiation of Posterior Fossa Ependymoma in the Molecular Era: A Retrospective Multicohort Analysis. J. Clin. Oncol. *34*, 2468–2477.

Ramírez, F., Ryan, D.P., Grüning, B., Bhardwaj, V., Kilpert, F., Richter, A.S., Heyne, S., Dündar, F., and Manke, T. (2016). deepTools2: a next generation web server for deep-sequencing data analysis. Nucleic Acids Res. *44* (W1), W160-5.

Ryall, S., Guzman, M., Elbabaa, S.K., Luu, B., Mack, S.C., Zapotocky, M., Taylor, M.D., Hawkins, C., and Ramaswamy, V. (2017). H3 K27M mutations are extremely rare in posterior fossa group A ependymoma. Childs Nerv. Syst. *33*, 1047–1051.

Saunders, C.T., Wong, W.S.W., Swamy, S., Becq, J., Murray, L.J., and Cheetham, R.K. (2012). Strelka: accurate somatic small-variant calling from sequenced tumor-normal sample pairs. Bioinformatics *28*, 1811–1817.

Shannon, P., Markiel, A., Ozier, O., Baliga, N.S., Wang, J.T., Ramage, D., Amin, N., Schwikowski, B., and Ideker, T. (2003). Cytoscape: a software environment for integrated models of biomolecular interaction networks. Genome Res. *13*, 2498–2504.

Sidoli, S., Bhanu, N.V., Karch, K.R., Wang, X., and Garcia, B.A. (2016). Complete Workflow for Analysis of Histone Post-translational Modifications Using

Bottom-up Mass Spectrometry: From Histone Extraction to Data Analysis. J. Vis. Exp. *111*, 54112.

Skene, P.J., and Henikoff, S. (2017). An efficient targeted nuclease strategy for high-resolution mapping of DNA binding sites. eLife *6*, 576.

Sørensen, B.S., Toustrup, K., Horsman, M.R., Overgaard, J., and Alsner, J. (2010). Identifying pH independent hypoxia induced genes in human squamous cell carcinomas in vitro. Acta Oncol. *49*, 895–905.

Stuart, T., Butler, A., Hoffman, P., Hafemeister, C., Papalexi, E., Mauck, W.M., 3rd, Hao, Y., Stoeckius, M., Smibert, P., and Satija, R. (2019). Comprehensive Integration of Single-Cell Data. Cell *177*, 1888–1902.e21.

Subramanian, A., Tamayo, P., Mootha, V.K., Mukherjee, S., Ebert, B.L., Gillette, M.A., Paulovich, A., Pomeroy, S.L., Golub, T.R., Lander, E.S., and Mesirov, J.P. (2005). Gene set enrichment analysis: a knowledge-based approach for interpreting genome-wide expression profiles. Proc. Natl. Acad. Sci. USA *102*, 15545–15550.

Thompson, Y.Y., Ramaswamy, V., Diamandis, P., Daniels, C., and Taylor, M.D. (2015). Posterior fossa ependymoma: current insights. Childs Nerv. Syst. *31*, 1699–1706.

Tian, Y., Morris, T.J., Webster, A.P., Yang, Z., Beck, S., Feber, A., and Teschendorff, A.E. (2017). ChAMP: updated methylation analysis pipeline for Illumina BeadChips. Bioinformatics *33*, 3982–3984.

Toustrup, K., Sørensen, B.S., Nordsmark, M., Busk, M., Wiuf, C., Alsner, J., and Overgaard, J. (2011). Development of a hypoxia gene expression classifier with predictive impact for hypoxic modification of radiotherapy in head and neck cancer. Cancer Res. *71*, 5923–5931.

Tyanova, S., Temu, T., Sinitcyn, P., Carlson, A., Hein, M.Y., Geiger, T., Mann, M., and Cox, J. (2016). The Perseus computational platform for comprehensive analysis of (prote)omics data. Nat. Methods *13*, 731–740.

Ulanovskaya, O.A., Zuhl, A.M., and Cravatt, B.F. (2013). NNMT promotes epigenetic remodeling in cancer by creating a metabolic methylation sink. Nat. Chem. Biol. *9*, 300–306.

Vladoiu, M.C., El-Hamamy, I., Donovan, L.K., Farooq, H., Holgado, B.L., Sundaravadanam, Y., Ramaswamy, V., Hendrikse, L.D., Kumar, S., Mack, S.C., et al. (2019). Childhood cerebellar tumours mirror conserved fetal transcriptional programs. Nature *572*, 67–73.

Walmsley, S.R., Chilvers, E.R., Thompson, A.A., Vaughan, K., Marriott, H.M., Parker, L.C., Shaw, G., Parmar, S., Schneider, M., Sabroe, I., et al. (2011). Prolyl hydroxylase 3 (PHD3) is essential for hypoxic regulation of neutrophilic inflammation in humans and mice. J. Clin. Invest. *121*, 1053–1063.

Wang, K., Li, M., and Hakonarson, H. (2010). ANNOVAR: functional annotation of genetic variants from high-throughput sequencing data. Nucleic Acids Res. *38*, e164.

Wei, T., and Simko, V. (2017). R package "corrplot": Visualization of a Correlation Matrix (Version 0.84). https://cran.r-project.org/web/packages/corrplot/corrplot.pdf.

Winter, S.C., Buffa, F.M., Silva, P., Miller, C., Valentine, H.R., Turley, H., Shah, K.A., Cox, G.J., Corbridge, R.J., Homer, J.J., et al. (2007). Relation of a Hypoxia Metagene Derived from Head and Neck Cancer to Prognosis of Multiple Cancers. Cancer Res. *67*, 3441–3449.

Witt, H., Mack, S.C., Ryzhova, M., Bender, S., Sill, M., Isserlin, R., Benner, A., Hielscher, T., Milde, T., Remke, M., et al. (2011). Delineation of Two Clinically and Molecularly Distinct Subgroups of Posterior Fossa Ependymoma. Cancer Cell *20*, 143–157.

Yuan, Z.-F., Sidoli, S., Marchione, D.M., Simithy, J., Janssen, K.A., Szurgot, M.R., and Garcia, B.A. (2018). EpiProfile 2.0: A Computational Platform for Processing Epi-Proteomics Mass Spectrometry Data. J. Proteome Res. *17*, 2533–2541.

Zhang, H., Badur, M.G., Divakaruni, A.S., Parker, S.J., Jäger, C., Hiller, K., Murphy, A.N., and Metallo, C.M. (2016). Distinct Metabolic States Can Support Self-Renewal and Lipogenesis in Human Pluripotent Stem Cells under Different Culture Conditions. Cell Rep. *16*, 1536–1547.

R Core Team (2014). R version 3.6.0 (The R Project for Statistical Computing).

Cell

Article

Metabolic Regulation of the Epigenome Drives Lethal Infantile Ependymoma

Graphical Abstract

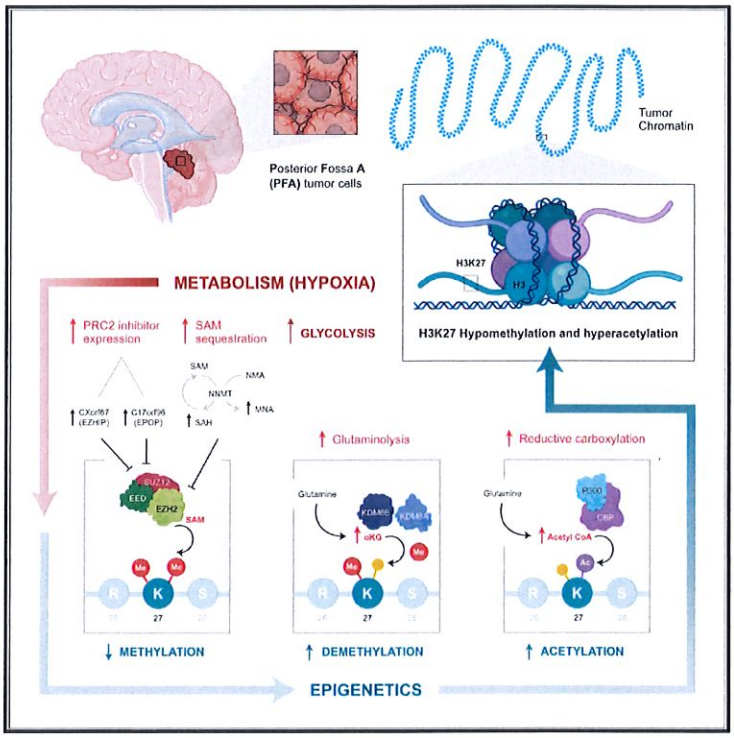

Highlights

- Hypoxic microenvironment is essential for propagation and growth of PFA ependymoma
- Hypoxia controls metabolic intermediates that maintain an H3K27 hypomethylated genome
- Inhibition or potentiation of histone lysine methylation diminishes PFA survival
- Gliogenic lineage of developing fetal hindbrain mirrors PFA metabolic alterations

Authors

Kulandaimanuvel Antony Michealraj, Sachin A. Kumar, Leo J.Y. Kim, ..., Sameer Agnihotri, Jeremy N. Rich, Michael D. Taylor

Correspondence

drjeremyrich@gmail.com (J.N.R.), mdt.cns@gmail.com (M.D.T.), sameer.agnihotri@gmail.com (S.A.), stephen.mack@bcm.edu (S.C.M.)

In Brief

Hypoxia reprograms the cellular metabolome and epigenome to promote growth of the most lethal ependymomas.

Michealraj et al., 2020, Cell *181*, 1329–1345
June 11, 2020
https://doi.org/10.1016/j.cell.2020.04.047

CellPress